8-2013

Evaluation of drug release from Abraxane and Doxil in tumor tissue.

Michael Christopher Clark
University of Louisville

EVALUATION OF DRUG RELEASE FROM ABRAXANE AND DOXIL IN TUMOR
TISSUE

By

Michael Christopher Clark
B.S., University of Louisville, 2012

A Thesis
Submitted to the Faculty of the
University of Louisville
J.B. Speed School of Engineering
as Partial Fulfillment of the Requirements
for the Professional Degree

MASTER OF ENGINEERING

Department of Bioengineering

August 2013

EVALUATION OF DRUG RELEASE FROM ABRAXANE AND DOXIL IN TUMOR
TISSUE

Submitted by:_____
Michael Christopher Clark

A Thesis Approved On

_____
Date

by the Following Reading and Examination Committee:
_____
Dr. Hermann Frieboes, Thesis Director

_____
Dr. Sethu

_____
Dr. Williams

ACKNOWLEDGMENTS

ABSTRACT

Currently, the clinical strategy to treat cancer consists of a combination of surgery, radiotherapy, and chemotherapy on the basis of clinical and molecular staging. Nanotechnology applied to biomedical sciences has paved the way for the development of novel strategies for early detection and more efficient treatment of diseases. Abraxane and Doxil are approved formulations that utilize nanoparticles carrying the drugs paclitaxel and doxorubicin, respectively; however, tumors are not completely eradicated in some patients. It is well known that inefficient vascularization may prevent optimal transport of oxygen, nutrients, and therapeutics to cells in solid tumors. In order to quantitatively evaluate therapy with Abraxane and Doxil, we apply a biocomputational cancer model to study nanoparticle drug release within tumor tissue. Both tumor cells and their microenvironment are represented in this model. Based on the specific characteristics of Abraxane and Doxil, we simulate drug release and diffusion at the tumor site. With the viable tumor region modeled as approximately 100 μm in diameter from blood vessels, and using IC_{50} data, the paclitaxel molecules of Abraxane were found to only penetrate 73 μm deep into the tumor, while although more efficient, doxorubicin molecules of Doxil only penetrate 93 μm of the tumor viable region. Therefore, we find that the modeling predicts that in the best case scenario, the drug concentrations delivered by these nanotherapies are insufficient to kill all of the tumor cells.

TABLE OF CONTENTS

LIST OF TABLES

LIST OF FIGURES

I.   INTRODUCTION

Cancer is a group of diseases characterized by abnormal cell growth. In this process, cells divide and form new cells when the body does not need them, and existing cells do not undergo apoptosis when they should. These mutated cells may in turn form a large mass of tissue, called a tumor. There are more than 100 different types of cancer, and they are typically named for the organ or type of cell in which they start, i.e. breast cancer. Cancer is widespread and it is estimated that 1,660,290 new cases will be diagnosed with 580,350 deaths due to cancer in the United States in 2013 [1]. Currently, the clinical strategy to treat cancer consists of a combination of surgery, radiotherapy, and chemotherapy on the basis of clinical and molecular staging [2]. Chemotherapy is the treatment of cancer with one or more cytotoxic antineoplastic drugs. Traditional chemotherapeutic agents kill cells that divide rapidly, without distinguishing between healthy and cancerous cells; therefore, normal healthy cells that are proliferating at a fast rate are targeted and eradicated as well, hence the cytotoxicity.

Treatment involving small molecules that are systemically injected tend to reach tumors at doses generally insufficient to eradicate the disease, since they tend to deposit non-specifically in almost any region perfused by blood [3]. However, recent developments in the field of nanotherapeutics have paved the way for drugs with reduced cytotoxicity and increased efficacy.

Conventional drug delivery methods include oral and intravenous (i.v.) routes and tend to exhibit dose-limiting toxicity [4]. Metabolic pathways of the body are easily

1

accessible by drugs through oral administration (i.e. tablets) and this can result in the drugs reaching and killing healthy tissue [4]. Specificity is the downfall of most drugs administered through a traditional i.v., which results in healthy tissue being mistaken as cancerous and this could lead to patient side effects such as neutropenia [4].

Nanomedicine is an emerging field in which nanotechnology is combined with medicine to deliver cures for patients. Nanotherapeutics is the use of nanomedicine in therapy. The efficacy of conventional chemotherapeutic agents is impaired mostly by their suboptimal accumulation at the tumor tissue. Nanoparticles are tiny objects engineered in laboratories to be sufficiently small to circulate safely within the vascular system. As such, many biomedical researchers have set their focus on nanoparticles for the development of novel strategies for early detection and more efficient treatment of diseases. In oncology, for example, chemotherapeutic agents have been reformulated into liposomes and nanoparticles which demonstrate improved pharmacokinetics and pharmacodynamics, and reduced off-target toxicity [3]. Tumor-targeting particles are typically spherical, with a diameter ranging between ~50 and 300 nm [3]. These diameters are chosen because they are optimal for transport through the bloodstream and into tumor tissue. Any smaller and a sufficient particle fraction may not accumulate in the tumor tissue due to diffusion and accumulation in other tissue sites. Any larger and the particles may not be able to diffuse from the vasculature and into tumor tissue. Two such combinations are currently on the market and in use clinically: Abraxane and Doxil.

Abraxane, developed by Araxis BioScience Inc., is a formulation of paclitaxel in which the drug is complexed with albumin to form stable, 130 nm particles [5]. Abraxane is currently used in the treatment of metastatic breast cancer. Before Abraxane, paclitaxel

had to be formulated with Cremphor®-EL, a version of polyethoxylated castor oil, and studies have shown that Cremphor®-EL can cause biological events that lead to acute hypersensitivity reactions and neurological toxicity when co-administered with paclitaxel through i.v. infusion [6]. The nanoparticle formulation of Abraxane eliminates the use of this toxic delivery vehicle, and replaces it with albumin, a protein found naturally in the blood plasma of humans. This allows a higher dose of paclitaxel to be delivered by Abraxane, eliminates solvent-related hypersensitivity reactions, results in more rapid clearance from the plasma with linear pharmacokinetics, and reduces neutropenia [5].

Doxil is a doxorubicin HCl liposome injection indicated for the treatment of patients with ovarian cancer whose disease has progressed or recurred after platinum-based chemotherapy [7]. However, studies have shown that Doxil is capable of inducing durable responses in metastatic breast cancer with unique pharmacokinetics and toxicity profiles [8]. Doxil has an average particle size of 87.3 nm [9]. Doxil reduces the cytotoxicity of doxorubicin by increasing the specificity and accumulation of doxorubicin within the tumor site. Doxil achieves this through its STEALTH® liposome drug encapsulation and delivery mechanism. These liposomes are microscopic vesicles with a phospholipid bilayer that are protected from detection by the mononuclear phagocyte system and have increased blood circulation time. The liposomes are formulated with surface-bound methoxypolyethylene glycol (MPEG), and it is this process of pegylation that protects the liposomes [7].

In vitro and *in vivo* studies have shed much light upon the mechanisms of drug delivery and uptake by cancerous tumor masses. However, despite much research, *in vitro* studies have not revealed every detail of the mechanisms. It is well known that

inefficient vascularization may prevent optimal transport of oxygen, nutrients, and therapeutics to cancer cells in solid tumors. In order to reach the total population of tumor cells, the drug must diffuse through the tumor tissue in its entirety. As such, there are diffusion gradients created by the dense tumor cells and there is evidence that suggests that these gradients may significantly limit drug dissemination throughout the tumor [10]. Oxidative stress and a decrease in the number of proliferating cells create physiologic resistance due to both hypoxia and hypoglycemia. These stresses, among others, can lead to a selection of apoptotic resistant cells. This evidence suggests that the diffusion process alone can lead to the evolution of drug resistance in tumor cells, exceeding predictions based on individual cell phenotype [10]. The quantification, with any clinical accuracy, of the resistance effects of diffusion gradients has been difficult. Biocomputational modeling of tumor drug response has been pursued to better understand this complex problem.

Previous studies have been conducted in which mathematical modeling and computer simulations were used to study the retention of nanoparticles within tumor vessels as a function of the tumor development stage [3, 10]. It was speculated that tumoritropic accumulation of nanoparticles could be affected by how developed the neovasculature and pre-existing vasculature are surrounding the tumor and by the expression of vascular receptor molecules on the nanoparticle surface. The affinity of the nanoparticles for the vessels was found to be a function of nanoparticle size, ligand density, as well as vascular receptor expression. For high vascular affinities, nanoparticles tend to accumulate mostly at the inlet tumor vessels leaving the inner and outer vasculature depleted of nanoparticles. For low vascular affinities, nanoparticles

distribute more uniformly intra-tumorally, but exhibit low accumulation doses. It was shown that an optimal vascular affinity could be identified through a balance between accumulation doses and uniform spatial distribution of the nanoparticles. The balance depends on the stage of tumor development (vascularity and endothelial receptor expression) and the nanoparticle properties (size, ligand density and ligand-receptor molecular affinity). The results enabled the selection of an optimal nanoparticle formulation presenting high accumulation doses and uniform spatial intra-tumor distributions as a function of the development stage of the malignancy. It was predicted that a moderate nanoparticle vascular affinity provides the proper balance between optimal spatial distribution and absolute tumoritropic accumulation [3].

II.   METHODS

The mathematical model used in this study represents both the tumor cells and their microenvironment. The mathematical model describes viable and necrotic tumor tissue, and diffusion of cell substrates and nanoparticles (small molecules), implementing the conservation of mass and momentum (as in [11]) in a 2-D Cartesian coordinate system. The initial condition of the model is a tumor with diameter <50 μm, in the middle of a pre-existing vasculature grid as shown in Figure 1 [3]. Growth is described as a function of total cycling cells and necrosis from hypoxia is calculated as a function of oxygen using the mass conservation equations. These equations are then combined with the diffusion of small molecules to obtain a reaction-diffusion equation. The rate constants for proliferation and apoptosis are spatiotemporally heterogeneous, as they depend on the availability of cell nutrients and oxygen. Published experimental data was used to calibrate the model parameters as in [10, 12-15]. The mathematical model was incorporated into a C++ (programming language) executable program that was used for tumor growth simulations. Figure 1 was generated using this program and setting a tumor growth time of 18 days. The main tumor model parameters as used in this computer program are summarized in Appendix I from [11]. Since the computer simulation is conducted in 2D, some of the parameters are simplified; as such, if a 3D simulation was desired, these parameters, such as characteristic tumor volume would need to be modified to incorporate this third dimension. 3D simulation is not reviewed in full detail, as it is beyond the scope of this study.
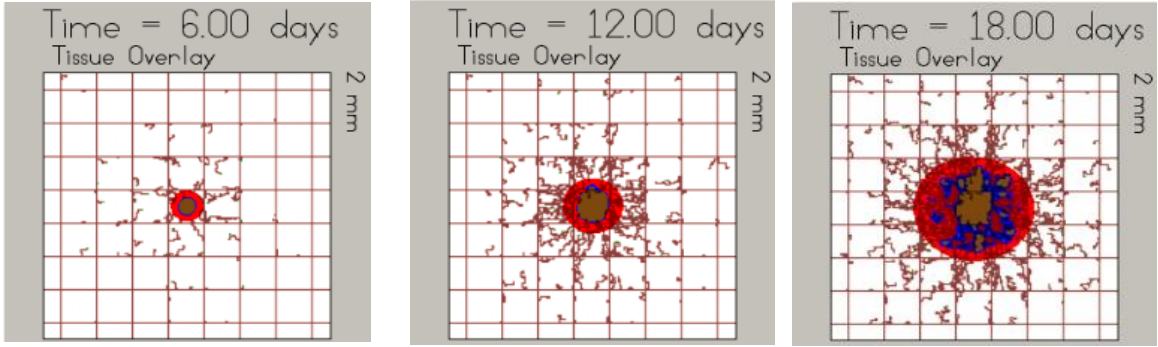
FIGURE 1- Output Of The Mathematical Model Showing Tumor Growth At Days 6, 12, and 18. Viable Tissue Is Red, Hypoxic Is Blue, And Necrotic Is Brown.

In order to more accurately express the spatiotemporal dynamics of solid tumor growth, conservation of momentum (due to tissue velocity as the tumor grows or shrinks) and physical transport (diffusion, advection, and convection of substances) were also incorporated into the model. Models of vessel growth, branching, and anastomosis [16], were coupled together with blood flow to model angiogenesis. The tumor vasculature acts as a source of oxygen, cell nutrients, and nanoparticles, and its inclusion to the model enables evaluation of the local effects of vascularization and blood flow on tumor cells and nanoparticle transport. This also expands knowledge of the micro-environment conditions such as hypoxia that lead to the development of intra-tumor heterogeneity [3].

To model tumor growth, the tumor region was denoted as Ω and its boundary as Σ [13]. The tumor was divided into three regions: proliferating, hypoxic, and necrotic. The proliferating region, denoted as Ω_P, is the area in which tumor cells have sufficient oxygen and nutrient levels for proliferation. The hypoxic region, Ω_H, is the portion of the tumor where oxygen and nutrient levels are sufficient for cell survival but cannot sustain proliferation. The necrotic region, Ω_N, is the inner portion of the tumor where oxygen and

nutrient levels are too low to maintain cellular viability and is mostly comprised of dead cells. A schematic of these three regions can be seen in Figure 2. A generalized Darcy's law gives the non-dimensional tumor velocity [13]:

$$v_c = -\mu \nabla P + \chi_E \nabla E \qquad \text{(Equation 1)}$$

here μ is the cell mobility as a function of adhesion of the cells to each other and to the matrix, P is oncotic pressure, χ_E is the haptotaxis coefficient, and E is the ECM density. The ECM is modeled as a non-diffusible matrix of macromolecules such as collagen and fibronectin. The growth of the tumor is associated with the rate of volume change by assuming that the density of cells is constant in the proliferating region, $\nabla \cdot v_c = \lambda_p$. The non-dimensional net proliferation rate, λ_p, is $\lambda_p = \sigma - A$ in Ω_P with σ as the concentration of oxygen and cell nutrients and A as the natural apoptosis rate. $\lambda_p = -G_N$ in Ω_N, where G_N is the non-dimensional rate of volume loss in the necrotic regions, with the assumption that fluid is removed and cellular debris is constantly degraded.
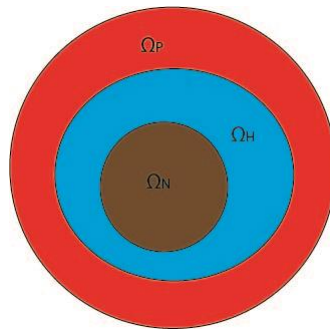

FIGURE 2- Generalized Schematic Of A Tumor, Showing The Proliferating Ω_P, Hypoxic Ω_H, And Necrotic Ω_N Cell Regions.

An angiogenesis model was included based on McDougall et al. (2006) [17] and coupled with the tumor growth model for tumor-induced angiogenesis. The angiogenesis

model accounts for blood flow through the vascular network, non-Newtonian effects, vascular leakage and vascular network remodeling due to wall shear stress and mechanical stresses generated by the developing tumor. A fundamental assumption of the model is that endothelial cells are stimulated to migrate based on chemotaxis due to tumor angiogenic factors (TAF) released by tumor hypoxic tissue, and haptotaxis due to gradients of extra-cellular matrix (ECM) along with random motility. The conservation of endothelial cells is described in a non-dimensional equation from [13]:

$$\frac{\partial n}{\partial t} = \nabla \cdot (D \nabla n) - \nabla (\chi_{sprout}^{T}(T) n \nabla T) - \nabla \cdot (\chi_{sprout}^{E} n \nabla E) \qquad \text{(Equation 2)}$$

where n is the non-dimensional endothelial cell density per unit area, and T and E are the TAF and ECM concentrations, respectively. The diffusion coefficient D represents random migration and is assumed constant. The chemotactic migration is described by χ_{sprout}^{T}, while the haptotactic migration is described by χ_{sprout}^{E}. In [13], a discretized and stochastic form of Equation 2 is given which details the displacement of individual endothelial cells at the tips of growing vascular sprouts. The blood flow was modeled by setting an inflow and outflow pressure [3]. As the tumor grows due to cell proliferation, it remodels the surrounding blood vessels. Some cells within the tumor become hypoxic after being pushed away from vessels by proliferating cells and in turn secrete angiogenic factors. These angiogenic factors lead to the creation of new vessels that eventually tie into the pre-existing vascular network and supply blood to these hypoxic cells.

When modeling the transport of small molecules s such as oxygen ($s = \sigma$), the assumption was made that the timescale for cell proliferation is much larger (~1 day) than the timescale for the diffusion of small molecules (~1 minute or less). This allowed the use of quasi-steady reaction-diffusion equations describing the transport of s in a model

[11] following previous work [13]. It is assumed that the pre-existing vasculature and the neo-vasculature supply small molecules at rates λ_{pre}^s and λ_{neo}^s, respectively. It is also assumed that the small molecules diffuse into normal and cancerous tissue with a constant diffusion coefficient D_s, are taken up by normal cells (with rate λ_{tissue}^s) and tumor cells (with rate λ_{tumor}^s in the proliferating region and q_s in the hypoxic region), and decay (with rate λ_N^s) in the necrotic region. The equations are:

$$0 = \nabla \bullet (D_s \nabla s) - \lambda^s(s)s + (\mathbf{x}, \mathrm{t}, \mathbf{1}_{vessel}, s) \qquad \text{(Equation 3)}$$

$$\lambda^s = \begin{cases} \lambda_{tissue}^s & outside\ \Omega \\ \lambda_{tumor}^s & in\ \Omega_p \\ q_s(s) & in\ \Omega_H \\ \lambda_N^s & in\ \Omega_N \end{cases} \qquad \text{(Equation 4)}$$

where q_s is generally a smooth interpolating function that matches λ_{tumor}^s between the proliferating and hypoxic tumor regions, and λ_N^s between the hypoxic and necrotic tumor regions; position in space is described by $\mathbf{x}$; t is time and $\mathbf{1}$ is the characteristic function of the vessels (i.e. $\mathbf{1}_{vessel}$ equals 1 at the location of the vessels and 0 otherwise) [3]. For the special case of oxygen ($s=\sigma$), the reader is referred to [3].

The computation of vessel radii is based on [11, 13, 17-19]. The initial value of all vessel radii is set to 6 microns as in [13]. The variation of the radius ΔR depends on the wall shear stress, the intravascular pressure, and the blood flow carrying the hematocrit. The reader is referred to [3] for a full discussion of vessel radius adaptation.

Vascular accumulation of blood-borne nanoparticles is mediated by the regulation of dislodging hydrodynamics forces and adhesive interactions that occur at the particle-cell boundary. A probability of adhesion P_a can be introduced to quantify the strength and

likelihood of firm adhesive interactions between a nanoparticle decorated with ligand molecules and a cell membrane expressing specific receptor molecules [3]. P_a depends on the nanoparticle properties (size, shape, surface density of ligands) and local vascular biophysical conditions (wall shear rate, surface density of receptors). For spherical particles, the number n of particles with diameter d adhering within a blood vessel with shear rate S can be written as [3]:

$$n = n_0 \alpha d^{\delta_1} \exp\left[-\beta\left(1 + \gamma d^{\delta_2}\right) S \right] \qquad \text{(Equation 5)}$$

where n_o is the number of particles exposed to the vessel walls and the parameters α, β and γ are, respectively, proportional to i) the surface density of receptors on the endothelial cells (m_r) and ligands on the particle (m_l), and the ligand-receptor affinity under zero external force (K_{A0}) ($\alpha \propto m_r\, m_l\, K_{A0}$); ii) the characteristic length scale of the ligand-receptor bond (χ), and the viscosity of water (μ) ($\beta \propto \chi\, \mu\, /(k_B T m_r)$); and iii) the inverse of the surface density of receptors [3]. The coefficients δ_1 (~ 0.45) and δ_2 (~ 1.57) are derived from the best fit of Equation (5) with the experimental data shown in Boso and colleagues [20]. For typical values of $m_r = 10_{12}$ #/m-2; $m_l = 10_{14}$ #/m-2 and K_A

$_0 = 10_{-14}$ m2, the parameter $\alpha = O(10_{12})$ m-2 [21, 22]. For lower ligand-receptor affinities, α is correspondingly lower. For typical values of $m_r = 10_{12}$ #/m-2, $\chi = 10_{-10}$ m-1 and $\mu = 10_{-3}$ Pa s-1, the parameter $\beta = O(10_{-4})$ m-2 s. The parameter $\gamma = O(10_4)$ m-δ2. A uniform concentration of NPs in the blood is assumed, with the maximum normalized to 1. Due to heterogeneities in the vascular flow, a heterogeneous spatio-temporal distribution of the particles within the tumor vasculature is also expected [3].

III.   RESULTS

The goal of this study was to calculate the amount of drug molecules released by Abraxane and Doxil nanoparticles that are present at the tumor site after injection, and then use this data to estimate the diffusion of the active drug molecules through the tumor tissue.

In order to achieve this goal, a particle fraction estimation of nanoparticles at the tumor site was obtained using data from Huo et al. In their study, Huo et al. reported the number of 100 nm gold nanoparticles per MCF-7 (a metastatic breast cancer cell line) tumor spheroid after 3 hours, 5.6_E08 [23]. Here it is assumed that the Abraxane and Doxil nanoparticles will behave similarly to the gold nanoparticles based on their shared feature of spherical shape with 100 nm diameter, and that as a best case scenario they diffuse uniformly through the tumor tissue. Tumor spheroids are cell cultures grown *in vitro* which represent avascular tissue regions (areas without blood vessels) [24]. In this study, these spheroids were used to model the tumor tissue around a tumor blood vessel. The total number of injected particles was estimated using the fact that 200 µL of particle solution was injected with a final concentration of 1 nmol/L. The volume of solution was multiplied by the concentration to obtain nanomoles of particles, and then this value was converted to moles and multiplied by Avogadro's number to obtain the total injected particles, 1.2044_E11. Huo et al. also provided bright field images of tumor spheroids, and these images were used to obtain an approximate diameter of 400 µm for tumor nodules

[23]. Assuming spherical geometry, we used this spheroid data to estimate the volume of tissue around a tumor blood vessel using Equation 6.

$$V = \frac{4}{3}\pi r^3$$
(Equation 6)

Subsequently, the volume of the necrotic region of the spheroid was calculated using the assumption that the viable portion of a tumor is only approximately 100 μm in diameter [10]. This viable region stems from experiments with spheroids that show that spheroids develop a layer, approximately 100 μm thick, of viable cells around a core of necrotic cells [25]. The necrotic region volume was then subtracted to obtain a viable tumor region volume, ~0.02 mm^3. The total number of particles and the number of particles per spheroid were then divided by this viable volume to obtain particles per mm^3. The number of particles per spheroid per volume was then divided by the total number of particles per volume to obtain the estimated tumor particle fraction used in this study, 2.8%. This particle fraction was then used to calculate the number of molecules of drug per tumor as described below.

In order to estimate the diffusion gradient of the drug molecules away from the nanoparticles and through the tumor tissue, a Bessel equation of the zeroth kind was used.

$$W_m(r) = J_0(k_m r) = J_0(\frac{\alpha_m}{R}r)$$
(Equation 7)

Equation 7 represents solutions of the Bessel equation that vanish at r = R. The parameters used were as follows: r is the distance away from the nanoparticle (0-100 μm), m is an integer constant that was set to 1 for the purpose of this study, R = diffusion penetration length from (Frieboes 2009) and is equal to 100 μm, J_0 denotes the Bessel function of the zeroth kind, α_m denotes zeros of J_0 and α_1 was given as 2.405, and $W_m(r)$

is equal to the amount of drug present. [26] Figure 3 below shows the data that was obtained using r = 0-100 μm with a step of 10 μm.

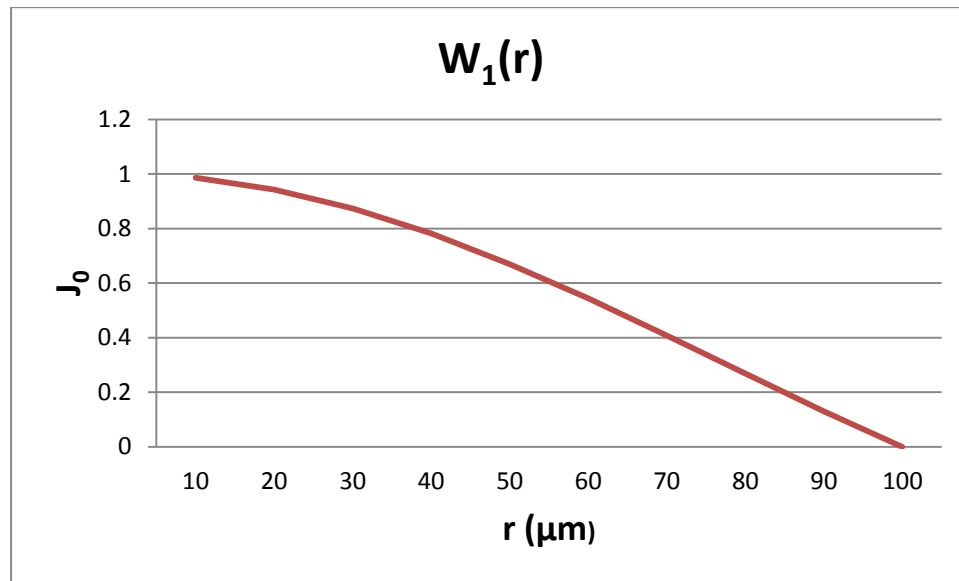FIGURE 3- Bessel Function Of The Zeroth Kind For r = 10-100 μm.

We modeled the diffusion of the drug molecules (paclitaxel and doxorubicin) through the tumor tissue as a gradient originating from a single nanoparticle (Abraxane and Doxil). The particle fraction per tumor area was combined with the Bessel function data to create gradient "bands" of drug diffusion within the tumor tissue as can be seen in Figure 4.
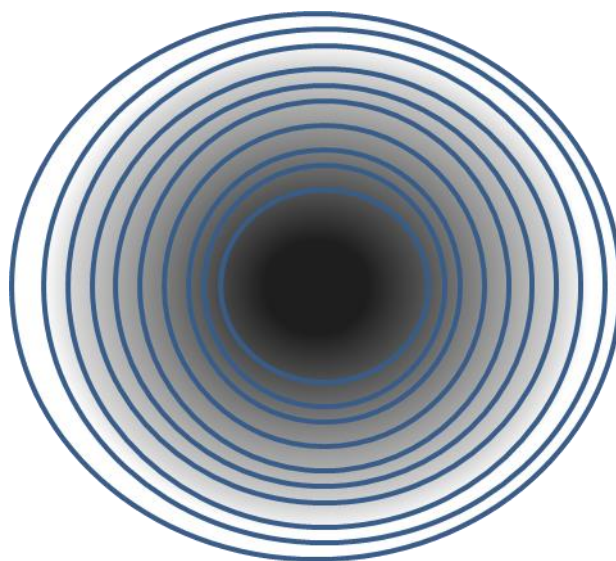
FIGURE 4- Schematic Of The Drug Diffusion Gradient Within Tumor Tissue Originating From A Single Drug Nanoparticle From High Concentration (Dark Color, Center) To Lowest (White At Periphery).

To do this, it was of interest to calculate the number of molecules of paclitaxel and doxorubicin per individual nanoparticle unit for Abraxane and Doxil, respectively. For both nanoparticles, it was assumed that the volume of plasma (V_P) in the human body is equal to approximately 3L. For Abraxane, two more assumptions had to be made. First, it was assumed that a person is 1.8 m^2 in area. This value, multiplied by recommended dosage of 260 mg/m^2, resulted in the amount of Abraxane per person- 468 mg/person [5]. From [27], Abraxane nanoparticles are 76% paclitaxel and multiplying this by the amount of Abraxane per person, there was found to be 356 mg paclitaxel per person. Consequently, the 112 mg left out of the 468mg is the amount of albumin per person. Using Avogadro's number and the molecular weights of albumin and paclitaxel, it was calculated that there is 1.02_E18 molecules of Albumin per person and 2.51_E20 molecules of paclitaxel per person. The ratio of these values was found to be 246.4 molecules of

paclitaxel per molecule of Albumin. It was assumed that there is 1 Albumin molecule per Abraxane particle based on light scattering data from [5]. Consequently, Abraxis Bioscience believes that Abraxane particles dissociate into individual albumin molecules that then circulate with paclitaxel still attached [5]. Using V_p of 3L and a C_{max} of 591 ng/mL, it was calculated that 1.25_E18 molecules of paclitaxel are present in the bloodstream after Abraxane injection [5]. Dividing this number by the number of molecules of paclitaxel per nanoparticle, 5.07_E15 nanoparticles of Abraxane present in the bloodstream was obtained. Given the vascularized nature of tumors, we then used this value as an approximation of the number of nanoparticles at the tumor site after injection.

Calculations for the number of molecules of Doxil present after injection into the bloodstream were similar to that of Abraxane. Using a C_{max} of 20.7 mg/L and V_p of 3L, it was calculated that there is 62.1 mg of Doxil in the bloodstream upon injection [8]. Converting this value to grams, dividing by the molecular weight of doxorubicin (543.5 g/mol), and then multiplying by Avogadro's number yields 6.88_E19 molecules of doxorubicin in the bloodstream. Next, given the fact that there are approximately 12.5 thousand molecules of doxorubicin per Doxil nanoparticle, it is calculated that there are 5.50_E15 nanoparticles of Doxil present in the bloodstream after injection at a dosage of 45 mg/m^2 [28]. As shown before for Abraxane, this number was then used as an approximation of the number of nanoparticles at the tumor site after injection.

Once obtained, the number of nanoparticles of Abraxane and Doxil were multiplied by the number of molecules of paclitaxel and doxorubicin, respectively, per nanoparticle to obtain 1.25_E18 molecules of paclitaxel and 6.88_E19 molecules of doxorubicin within the tumor tissue after injection. These values were then multiplied by

the 0.0279 particle fraction per tumor to obtain 3.4854_E16 molecules paclitaxel per tumor and 1.9181_E18 molecules of doxorubicin per tumor. After that, the values were multiplied by the Bessel data for each gradient band, then divided by Avogadro's number and multiplied by the respective molecular weight for each drug to obtain Figures 5, and 6 which describe grams of drug per tumor as a function of distance from the particles.
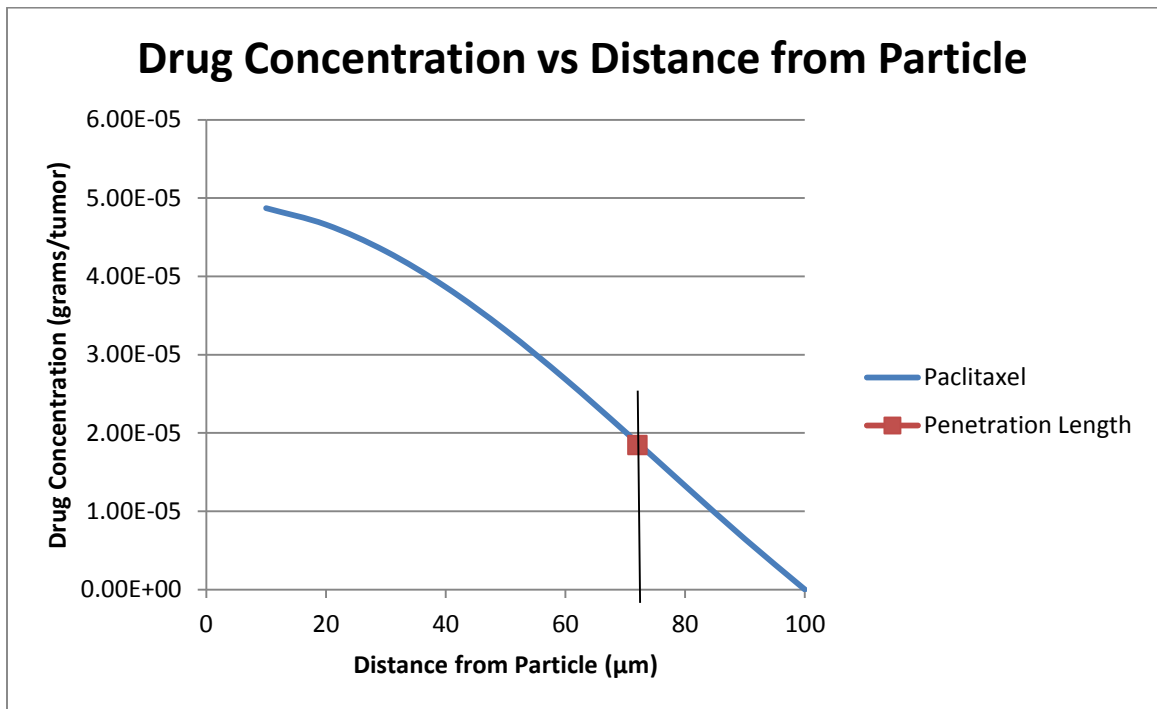
FIGURE 5- Drug Per Tumor Versus Distance From Particle For Active Drug In

Abraxane (Paclitaxel).
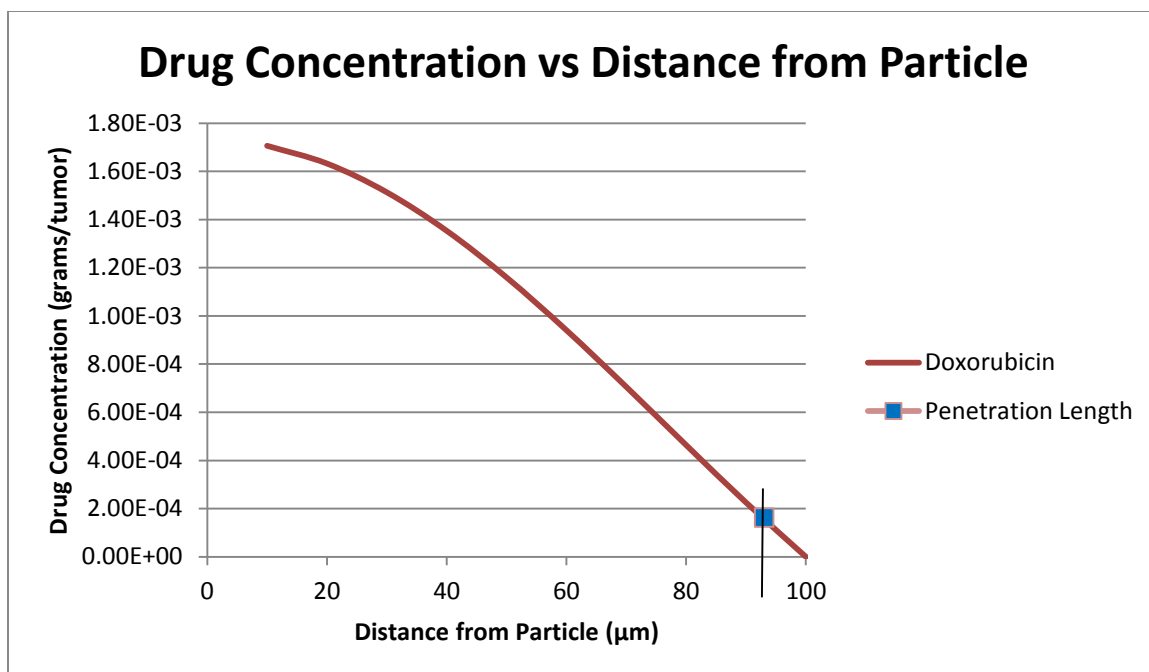
FIGURE 6- Drug Per Tumor Versus Distance From Particle For Active Drug In Doxil
(Doxorubicin).

In addition, the 50% inhibitory concentration (IC_{50}), or the concentration of drug needed to induce apoptosis in 50% of a given cell population, was found in the literature for both paclitaxel and doxorubicin when used for the *in vitro* treatment of MCF-7 breast cancer cells. The values were found to be 7.2 nM/L and 100 nM/L for paclitaxel [29] and doxorubicin [30], respectively. These values were used to approximate the penetration length of the drugs into the tumor, since they represent a best case scenario of drug performance. For the approximation, the values were converted to grams of drug in the plasma and then fitted to their respective curves in Figures 5 and 6 to obtain the penetration lengths (72 μm for paclitaxel and 93 μm for doxorubicin) found in Table I.

TABLE I

DRUG CONCENTRATION (GRAMS) VERSUS DISTANCE FROM PARTICLE

Drug	Grams Drug in Plasma	Penetration Length (μm)
Doxorubicin	1.6306E-04	93
Paclitaxel	1.8444E-05	72

IV.   DISCUSSION

Nanomedicine has greatly improved the chances of successfully killing cancer and increasing the lifespan of cancer patients; however, as seen in Table I, current nanoparticle delivery systems are still not 100% efficient. Abraxane particles only achieve 50% cell apoptosis in about 72% of the tumor, and although more efficient, Doxil particles only achieve that value in 93% of the tumor. Substantial portions of tumor tissue are predicted to survive when these drugs are used, even in the best case scenario of optimal drug action as occurs *in vitro*. We assume uniform distribution of the particles within the tumor tissue, so that overlapping of drug diffusing from adjacent particles is minimal; even without this assumption of homogeneity, it is reasonable to assume that at the tissue scale the effect of overlapping drug release would be balanced by areas where drug concentration is minimized, leading to heterogeneous drug concentration and hence sub-optimal tumor dosing as is predicted by modeling [2] and experiments *in vivo* [31].

In vitro analysis of nanoparticle transport within tumor spheroids was conducted by Gao et al. using pharynx FaDu cells. In this study, near-neutral zwitterionic hydrogenated soy phosphatidylcholine (HSPC) liposomes sterically stabilized with pegylation were prepared and characterized. The liposomes were found to have a similar diameter (approximately 110 nm) to the nanoparticles modeled in this study and the spheroids used also had a similar diameter of 325 μm [32]. After 2 hours of tumor treatment with the nanoparticles, they found that the HSPC particles only penetrated approximately 40 μm from the tumor periphery into the center [32]. The results of their

study agree with ours in that there is limited penetration by nanoparticles of approximately 100 nanometers in diameter. Further, due to this penetration barrier, substantial portions of tumors are not being killed during cancer treatment.

In a study by Lankelma et al., ten patients were treated with locally advanced breast cancer with doxorubicin i.v. Through tumor biopsy and fluorescence methods, they found that doxorubicin gradients occurred in tumor islets with high concentrations in the periphery and low concentrations in the center of the islets [33]. Two hours post injection, Lankelma et al. found that doxorubicin only penetrated a maximum of approximately 40 μm into the tumor islet core. Our results show that nanoparticle delivery of doxorubicin significantly increases tumor penetration *in vivo*, yet there are still portions of tumors that are not eradicated.

Primeau et al. extended the work of Lankelma et al. to reinforce the notion that chemotherapy with DNA-binding drugs such as doxorubicin is limited by poor penetration through tumor tissue [34]. They studied the diffusion of doxorubicin from blood vessels in mice. They prepared their tumors using mouse mammary sarcoma EMT6 and the mouse mammary adenocarcinoma 16C. Using fluorescent imaging, they found that doxorubicin concentrations seemed to be highly localized around tumor blood vessels [34]. Primeau et al. report a characteristic penetration length (away from blood vessels and into the tumor) of 50 μm for doxorubicin, beyond which their results suggest that viable cells exist and do not receive enough drug to cause toxicity [34]. While this experiment was not conducted using human cells, it gives good insight into the diffusion of doxorubicin *in vivo*.

These results and our study confirm that the diffusion of doxorubicin and other small molecules is hampered in tumor tissue. For cancer treatment, 100% efficiency must be achieved to guarantee long-term patient survival. By modeling drug diffusion based on particle penetration into tumors, this work creates a quantitative approach that could be used to predict tumor viability based on penetration depth of drug particles, and thus help to improve treatment outcome.

For instance, direct patient benefit from therapy with these drugs could be calculated. If one had a sample of the patient's tumor cells, an IC_{50} assessment for each drug could be performed. Then one could follow the aforementioned methods to calculate the grams of drug per tumor that would arise from these IC_{50} values that could be plotted on Figures 5 and 6, respectively, to approximate a drug penetration length. An example of these calculations can be found in Appendix II. This penetration length, whether low or high, would indicate whether Abraxane or Doxil would be an effective method of cancer treatment for this particular patient.

Physiological Name	Parameter	Scaled by or Unit	Values
oxygen diffusion	D_σ	D_σ^*, a characteristic dimensional	1.0
characteristic value of	$\overline{H}_D$	unit as a fraction	0.45
discharge haematocrit			
minimal value needed	$\overline{h}_{min}$	unit as a fraction	0.0
for oxygen extravasation			
coefficient		oxygen diffusion coefficient	
rate of cell mitosis	λ_M	unit: per s	0.77e-5
characteristic volume	V_T	unit: μm^3	1000
uptake rate of oxy-		λ_σ^*, the characteristic rate of	1.5
gen in proliferating	λ_{prolif}^σ	oxygen uptake in the	
tumor region		proliferating tumor region	
uptake rate of oxygen in	λ_{host}^σ	λ_σ^*	0.12
host microenvironment			
uptake rate of oxygen in	λ_{hyp}^σ	λ_σ^*	1.3
hypoxic tumor region			
decay rate of oxygen in	λ_{nec}^σ	λ_σ^*	0.35
necrotic tumor region			
baseline rate of oxygen	$\overline{\lambda}_{vasc}^\sigma$	λ_σ^*	0.25
transfer from vessels			
TAF diffusion coefficient	D_T	D_σ^*	0.005
production rate of by TAF	$\overline{\lambda}_{prod.}^T$	λ_σ^*	1.0
hypoxic tumor cells			
natural decay rate of TAF	$\overline{\lambda}_{decay}^T$	λ_σ^*	0.001
rate of binding	$\overline{\lambda}_{binding}^T$	λ_σ^*	0.006
by vessel tips			
minimum value of ECM	$\overline{E}_{mincutoff}^\chi$	E^*, the concentration of ECM	0.1
used in haptotaxis coefficient		secreted by tumor cells	
maximum value of ECM	$\overline{E}_{maxcutoff}^\chi$	χ_E^*	0.9
used in haptotaxis coefficient			
minimum haptotaxis rate	$\overline{\chi}_{E,min}$	$\chi_E^* E^*/l^2 \lambda_M$	0.0
maximum haptotaxis rate	$\overline{\chi}_{E,max}$	$\chi_E^* E^*/l^2 \lambda_M$	0.25
apoptosis rate	A	unit: per day	0
necrosis rate	G_N	unit: per day	0.2
tumor aggresiveness rate	G	unit: per day	26.8
MDE diffusion coefficient	D_M	$\lambda_M l^2$, where l is the length scale	1.0
production rate of MDE	$\overline{\lambda}_{prod.}^M$	λ_M	100.0
by tumor cells			
natural decay rate of MDE	$\overline{\lambda}_{decay}^M$	λ_M	10.0
production rate of MDE	$\overline{\lambda}_{spr.prod.}^M$	λ_M	1.0
by vessel tips			
rate of production of	$\overline{\lambda}_{prod.}^E$	λ_M	2.72
ECM by tumor cells			
rate of production of	$\overline{\lambda}_{spr.prod.}^E$	λ_M	0.1
ECM by vessel tips			
rate of degradation of	$\overline{\lambda}_{degradation}^E$	$1/M^*$	1.0
ECM by MDE			
minimum value of ECM	$\overline{E}_{mincutoff}^\mu$	E^*	0.0
used in mobility coefficient			
maximum value of ECM	$\overline{E}_{maxcutoff}^\mu$	E^*	1.0
used in mobility coefficient			
minimum tumor mobility	$\overline{\mu}_{min}$	μ^*	1.0
maximum tumor mobility	$\overline{\mu}_{max}$	μ^*	4.0

FIGURE 7- Parameters Used In Computer Model from [11].

Sample IC$_{50}$ Calculation

1. First, an IC$_{50}$ assessment is performed on a patient's cells after a tumor biopsy
   using doxorubicin.

   The assessment yields an IC$_{50}$ equal to 80 nM/L.

2. Then, this value must be converted to moles of drug in the blood plasma using
   $V_P = 3L$.

   $(8.0_{E}\text{-}08\text{mol/L}) * 3L = 2.40_{E}\text{-}07$ mol Doxorubicin in Plasma

3. This value is then converted to grams of drug in the plasma.

   $(2.40_{E}\text{-}07\text{mol}) * (543.51926\text{g/mol}) = 1.30_{E}\text{-}04$ grams Doxorubicin in the plasma

4. Finally, this value is plotted on Figure 6, Drug Concentration vs. Distance From
   Particle for Doxorubicin, to find the estimated drug penetration length of the drug
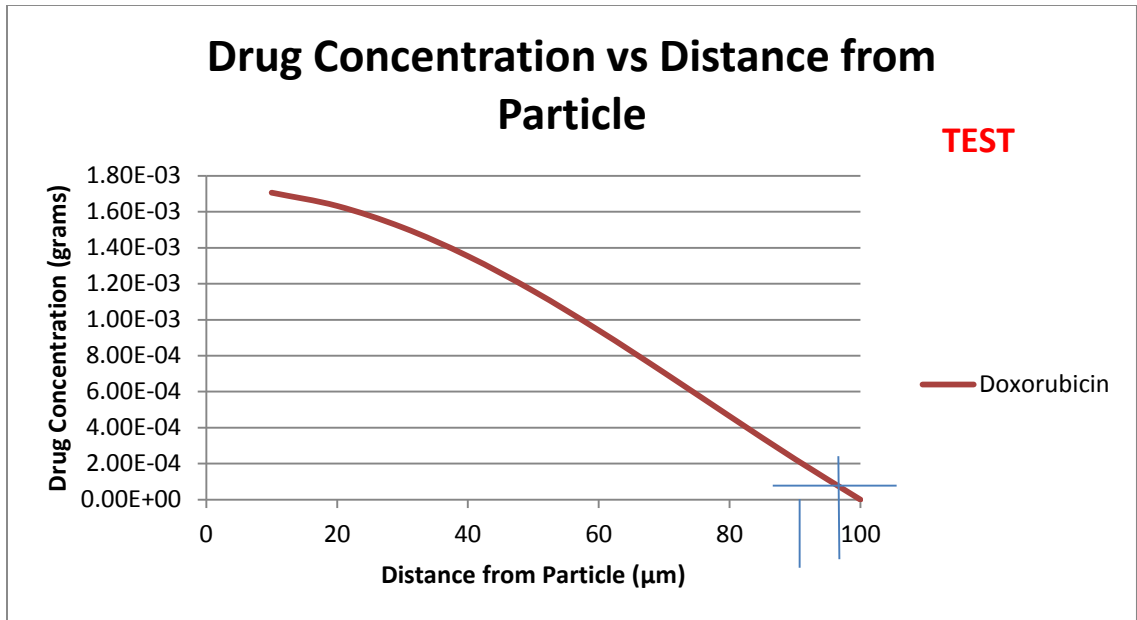   into the tumor tissue from a nanoparticle.

Figure 8- Penetration Length Estimation For Doxorubicin.

For this particular example, the penetration length would be equal to approximately 96 μm.

5. With this value, we can estimate that doxorubicin could eradicate almost 50% of the tumor tissue for the patient and may thus be a good drug option for the patient's chemotherapy treatment. Note, we say as much as since the estimated penetration length is for the best case scenario of drug treatment *in vitro*.

REFERENCES

1.   Society, A.C., *American Cancer Society: Cancer Facts and Figures 2013.* 2013.
2.   Frieboes, H.B., et al., *Physical oncology: a bench-to-bedside quantitative and predictive approach.* Cancer Res, 2011. **71**(2): p. 298-302.
3.   Frieboes, H.B., et al., *A computational model for predicting nanoparticle accumulation in tumor vasculature.* PLoS One, 2013. **8**(2): p. e56876.
4.   Sinha, R., et al., *Nanotechnology in cancer therapeutics: bioconjugated nanoparticles for drug delivery.* Mol Cancer Ther, 2006. **5**(8): p. 1909-17.
5.   Abraxis BioScience, I., *Abraxane ODAC Briefing Package*, 2006.
6.   Gelderblom, H., et al., *Cremophor EL: the drawbacks and advantages of vehicle selection for drug formulation.* Eur J Cancer, 2001. **37**(13): p. 1590-8.
7.   Ben Venue Laboratories, I., *Doxil Product Information*, 2012.
8.   Lyass, O., et al., *Correlation of toxicity with pharmacokinetics of pegylated liposomal doxorubicin (Doxil) in metastatic breast carcinoma.* Cancer, 2000. **89**(5): p. 1037-47.
9.   Bao, A., et al., *Direct 99mTc labeling of pegylated liposomal doxorubicin (Doxil) for pharmacokinetic and non-invasive imaging studies.* J Pharmacol Exp Ther, 2004. **308**(2): p. 419-25.
10.   Frieboes, H.B., et al., *Prediction of drug response in breast cancer using integrative experimental/computational modeling.* Cancer Res, 2009. **69**(10): p. 4484-92.
11.   Wu, M., et al., *The effect of interstitial pressure on tumor growth: coupling with the blood and lymphatic vascular systems.* J Theor Biol, 2013. **320**: p. 131-51.
12.   Frieboes, H.B., et al., *An integrated computational/experimental model of tumor invasion.* Cancer Res, 2006. **66**(3): p. 1597-604.
13.   Macklin, P., et al., *Multiscale modelling and nonlinear simulation of vascular tumour growth.* J Math Biol, 2009. **58**(4-5): p. 765-98.
14.   Pham, K., et al., *Predictions of tumour morphological stability and evaluation against experimental observations.* J R Soc Interface, 2011. **8**(54): p. 16-29.
15.   Sinek, J.P., et al., *Predicting drug pharmacokinetics and effect in vascularized tumors using computer simulation.* J Math Biol, 2009. **58**(4-5): p. 485-510.
16.   Anderson, A.R. and M.A. Chaplain, *Continuous and discrete mathematical models of tumor-induced angiogenesis.* Bull Math Biol, 1998. **60**(5): p. 857-99.
17.   McDougall, S.R., A.R. Anderson, and M.A. Chaplain, *Mathematical modelling of dynamic adaptive tumour-induced angiogenesis: clinical implications and therapeutic targeting strategies.* J Theor Biol, 2006. **241**(3): p. 564-89.
18.   McDougall, S.R., et al., *Mathematical modelling of flow through vascular networks: implications for tumour-induced angiogenesis and chemotherapy strategies.* Bull Math Biol, 2002. **64**(4): p. 673-702.
19.   Pries, A.R., T.W. Secomb, and P. Gaehtgens, *Structural adaptation and stability of microvascular networks: theory and simulations.* Am J Physiol, 1998. **275**(2 Pt 2): p. H349-60.
20.   Boso, D.P., et al., *Optimizing particle size for targeting diseased microvasculature: from experiments to artificial neural networks.* Int J Nanomedicine, 2011. **6**: p. 1517-26.
21.   Decuzzi, P. and M. Ferrari, *The adhesive strength of non-spherical particles mediated by specific interactions.* Biomaterials, 2006. **27**(30): p. 5307-14.
22.   Caputo, K.E. and D.A. Hammer, *Effect of microvillus deformability on leukocyte adhesion explored using adhesive dynamics simulations.* Biophys J, 2005. **89**(1): p. 187-200.

23. Huo, S., et al., *Superior penetration and retention behavior of 50 nm gold nanoparticles in tumors.* Cancer Res, 2013. **73**(1): p. 319-30.

24. Ward, J.P. and J.R. King, *Mathematical modelling of drug transport in tumour multicell spheroids and monolayer cultures.* Math Biosci, 2003. **181**(2): p. 177-207.

25. Sutherland, R.M., *Cell and environment interactions in tumor microregions: the multicell spheroid model.* Science, 1988. **240**(4849): p. 177-84.

26. Kreyszig, E., *Advanced engineering mathematics*. 8th ed. 1999, New York: Wiley.

27. Abraxis BioScience, I., *Abraxane Product Information*, 2013.

28. Martin, F., *Liposomes: Critical Formulation Parameters*, ALZA Corporation.

29. Nakayama, S., et al., *Prediction of paclitaxel sensitivity by CDK1 and CDK2 activity in human breast cancer cells.* Breast Cancer Res, 2009. **11**(1): p. R12.

30. Fornari, F.A., et al., *Interference by doxorubicin with DNA unwinding in MCF-7 breast tumor cells.* Mol Pharmacol, 1994. **45**(4): p. 649-56.

31. van de Ven, A.L., et al., *Integrated intravital microscopy and mathematical modeling to optimize nanotherapeutics delivery to tumors.* AIP Adv, 2012. **2**(1): p. 11208.

32. Gao, Y., et al., *Predictive Models of Diffusive Nanoparticle Transport in 3-Dimensional Tumor Cell Spheroids.* AAPS J, 2013.

33. Lankelma, J., et al., *Doxorubicin gradients in human breast cancer.* Clin Cancer Res, 1999. **5**(7): p. 1703-7.

34. Primeau, A.J., et al., *The distribution of the anticancer drug Doxorubicin in relation to blood vessels in solid tumors.* Clin Cancer Res, 2005. **11**(24 Pt 1): p. 8782-8.

VITA

Michael Clark received his Bachelor of Science in Bioengineering with high honors from the University of Louisville in 2012 in his hometown of Louisville, Kentucky. He is currently employed full time at a local engineering company in Louisville. He completed a Master of Engineering degree in Bioengineering at the University of Louisville under Dr. Hermann Frieboes, graduating with high honors.